A Multi-Level Spectral Model. I. Formulation and Hemispheric Integrations

WILLIAM BOURKE

Australian Numerical Meteorology Research Centre, Melbourne, Australia 3001

(Manuscript received 5 March 1974, in revised form 6 August 1974)

ABSTRACT

The formulation of a multi-level spectral model suitable for simulation of atmospheric flow on a hemispheric or global scale is presented. The derived primitive equations are employed together with spectral-grid transform procedures in the multi-level domain. An efficient semi-implicit time integration scheme is detailed and results of numerical integrations initialized from analytic fields and Southern Hemisphere data sets are presented.

A simple initializing device of divergence dissipation is suggested and shown to be most effective in eliminating spurious large-scale inertia-gravity oscillations.

1. Introduction

A numerical model of atmospheric flow is being developed to study global-scale dynamics and numerical weather prediction. The dynamic variables of the primitive meteorological equations are specified spectrally in the horizontal at each vertical level. The model is formulated in terms of the derived primitive equations extending the author's earlier formulation (Bourke, 1972, subsequently denoted as I). The model development has followed from the recent emergence of efficient methods of spectral multiplication as described by Orszag (1970) and Eliasen *et al.* (1970). The improved efficiency arises from the use of spectral grid transforms.

The spectral method has been commonly invoked to integrate filtered baroclinic models of the atmosphere: Kikuchi (1969) and Baer and Alyea (1971), for example. Robert (1966) applied the spectral method to a multilevel primitive equation model avoiding the complexity of interaction coefficients by use of modified harmonic functions. The advent of spectral grid transform procedures has now enlarged the capability and potential of the spectral method and at the present time several research groups are developing primitive equation spectral models employing these transform algorithms; Machenhauer and Daley (1972) are currently developing a primitive equation model incorporating a spectral representation in the vertical thereby generalizing to three dimensions their earlier formulation (Machenhauer and Rasmussen, 1972).

The present study demonstrates the efficiency and capability of the spectral method in modeling the atmosphere as a multilayered fluid on the sphere. The formulation of a model pertaining to a dry, adiabatic fluid considered at five vertical levels is presented together with details of an algorithm for implementing semi-implicit integration of the model. The model behavior with respect to both the usual diagnostic integrals and its predictive capability in the Southern Hemisphere are discussed. A simple initializing procedure has been developed and its performance is compared to other techniques.

2. Model formulation

The dynamics of the dry adiabatic atmospheric fluid may be described in terms of the following equations for momentum, thermodynamics, continuity and the hydrostatic relation

$$\frac{d\mathbf{V}}{dt}=-f\mathbf{k}\times\mathbf{V}-\nabla\Phi-RT\nabla\ln p_*+\mathbf{F} \tag{1}$$

$$\frac{dT}{dt}=\frac{RT}{c_p}\left(\frac{\dot\sigma}{\sigma}-\frac{\partial\dot\sigma}{\partial\sigma}-\nabla\cdot\mathbf{V}\right) \tag{2}$$

$$\frac{d\ln p_*}{dt}=-\nabla\cdot\mathbf{V}-\frac{\partial\dot\sigma}{\partial\sigma} \tag{3}$$

and

$$\frac{\partial\Phi}{\partial\sigma}=-\frac{RT}{\sigma}. \tag{4}$$

Here the vertical coordinate system of Phillips is employed; the vertical coordinate being defined as $\sigma=p/p_*$ where p_* denotes the surface pressure and p the pressure within the atmospheric fluid. $\mathbf{V}$ is the horizontal wind vector with eastward and northward components of u and v respectively, T is the absolute temperature, Φ is the geopotential height, f is the

Coriolis parameter, R is the gas constant for dry air, $\mathbf{F}$ is the horizontal frictional force, $\mathbf{k}$ is the vertical unit vector, ∇ is the horizontal gradient operator, $\dot{\sigma}$ is the total time derivative of σ, c_p is the specific heat at constant pressure for dry air and d/dt is the total time derivative.

The formulation of I is now paralleled in the following. The prognostics for the vertical component of relative vorticity and the horizontal divergence are found to be

$$\frac{\partial \xi}{\partial t} = -\nabla\cdot(\xi+f)\mathbf{V} - \mathbf{k}\cdot\nabla\times\left(RT'\nabla q + \dot{\sigma}\frac{\partial \mathbf{V}}{\partial \sigma} + \mathbf{F}\right) \tag{5}$$

$$\frac{\partial D}{\partial t} = \mathbf{k}\cdot\nabla\times(\xi+f)\mathbf{V} - \nabla\cdot\left(RT'\nabla q + \dot{\sigma}\frac{\partial \mathbf{V}}{\partial \sigma} + \mathbf{F}\right) - \nabla^2(\Phi' + RT_0 q + \tfrac{1}{2}\mathbf{V}\cdot\mathbf{V}). \tag{6}$$

The thermodynamic and continuity equations similarly expanded are

$$\frac{\partial T}{\partial t} = -\nabla\cdot\mathbf{V}T' + T'D + \dot{\sigma}\gamma - \frac{RT}{c_p}\left(D + \frac{\partial \dot{\sigma}}{\partial \sigma}\right) \tag{7}$$

$$\frac{\partial q}{\partial t} = -D - \frac{\partial \dot{\sigma}}{\partial \sigma} - \mathbf{V}\cdot\nabla q. \tag{8}$$

Here ξ is the vertical component of relative vorticity $k\cdot\nabla\times\mathbf{V}$, D is the horizontal divergence $\nabla\cdot\mathbf{V}$, q denotes $\ln p_*$, γ is the static stability defined as $RT/\sigma c_p - \partial T/\partial\sigma$. The subscripted zero denotes a horizontal mean value and the superscripted prime the deviation from that mean.

Upon defining the wind vector $\mathbf{V}$ in terms of a streamfunction ψ and a velocity potential χ as

$$\mathbf{V} = \mathbf{k}\times\nabla\psi + \nabla\chi, \tag{9}$$

the quantities ξ and D are seen to be expressible as

$$\xi = \mathbf{k}\cdot\nabla\times\mathbf{V} = \nabla^2\psi,$$
$$D = \nabla\cdot\mathbf{V} \quad = \nabla^2\chi.$$

Vertical integration of the continuity equation with boundary conditions $\dot{\sigma}=0$ at $\sigma=1$ and $\sigma=0$ yields the prognostic

$$\frac{\partial q}{\partial t} = \overline{D} + \overline{\mathbf{V}}\cdot\nabla q \tag{10}$$

and the diagnostic

$$\dot{\sigma} = \{(1-\sigma)\overline{D} - \overline{D}^{\sigma}\} + \{(1-\sigma)\overline{\mathbf{V}} - \overline{\mathbf{V}}^{\sigma}\}\cdot\nabla q, \tag{11}$$

where

$$\overline{(\ )} = \int_{\sigma=1}^{0}(\ )\partial\sigma \quad \text{and} \quad \overline{(\ )}^{\sigma} = \int_{\sigma=1}^{\sigma}(\ )\partial\sigma. \tag{12}$$

With the further substitutions $U = u\cos\phi$, $V = v\cos\phi$, Eqs. (5) to (8) may be expanded in part into spherical polar coordinates yielding, where λ denotes longitude, ϕ denotes latitude and a the radius is taken to be constant

$$\frac{\partial}{\partial t}\nabla^2\psi = -\frac{1}{a\cos^2\phi}\left(\frac{\partial A}{\partial \lambda} + \cos\phi\frac{\partial B}{\partial \phi}\right) - 2\Omega\left(\sin\phi\nabla^2\chi + \frac{V}{a}\right) \tag{13}$$

$$\frac{\partial}{\partial t}\nabla^2\chi = \frac{1}{a\cos^2\phi}\left(\frac{\partial B}{\partial \lambda} - \cos\phi\frac{\partial A}{\partial \phi}\right) + 2\Omega\left(\sin\phi\nabla^2\psi - \frac{U}{a}\right) - \nabla^2(E + \Phi' + RT_0 q) \tag{14}$$

$$\frac{\partial T}{\partial t} = -\frac{1}{a\cos^2\phi}\left(\frac{\partial}{\partial \lambda}UT' + \cos\phi\frac{\partial}{\partial \phi}VT'\right) + T'\nabla^2\chi + \gamma\dot{\sigma} + \frac{RT}{c_p}\{\overline{\nabla^2\chi} + (\mathbf{V}+\overline{\mathbf{V}})\cdot\nabla q\} \tag{15}$$

$$\frac{\partial q}{\partial t} = \overline{\mathbf{V}}\cdot\nabla q + \overline{\nabla^2\chi}. \tag{16}$$

Here

$$A = \xi U + \dot{\sigma}\frac{\partial V}{\partial \sigma} + \frac{RT'}{a}\cos\phi\frac{\partial q}{\partial \phi} - \frac{g}{p_*}\frac{\partial \tau_y}{\partial \sigma}, \tag{17}$$

$$B = \xi V - \dot{\sigma}\frac{\partial U}{\partial \sigma} - \frac{RT'}{a}\frac{\partial q}{\partial \lambda} + \frac{g}{p_*}\frac{\partial \tau_x}{\partial \sigma}, \tag{18}$$

$$E = \frac{U^2+V^2}{2\cos^2\phi}. \tag{19}$$

The frictional force $\mathbf{F}$ in (5) and (6) has been specified here to describe only vertical momentum transport at the surface; horizontal stresses τ_x and τ_y are specified as below in a conventional manner at the surface and in an attempt to describe the turning of the wind in the lowest model layer have an associated angle of turn α with respect to the direction of flow at the lowest model level. (A $\sin\phi$ latitudinal weighting reduces the influence of turning to zero at the equator; this is especially appropriate in hemispheric integrations where it would be inappropriate to consider turning of the wind at the equatorial wall. Without this $\sin\phi$ weighting global integrations initialized with identical flow in each hemisphere will lose their cross equatorial symmetry.)

Accordingly, τ_x and τ_y at the lower boundary are

specified as

$$\tau_x = -\frac{p_*}{RT_*} C_d \sqrt{2E}\{U\cos\alpha - V\sin\alpha\sin\phi\}$$

$$\tau_y = -\frac{p_*}{RT_*} C_d \sqrt{2E}\{V\cos\alpha + U\sin\alpha\sin\phi\}. \quad (20)$$

Here the subscript asterisk denotes the surface value and T_* is obtained via logarithmic extrapolation from the first two full levels. U, V, and $\sqrt{E}$ are taken to have the values of the lowest full level in the model. Within the fluid, τ_x and τ_y are taken to be zero. The values of coefficient of surface drag $C_d = 0.002$ and $\alpha = 20°$ have been employed in this study. [If in (20) the values preceding the bracket are taken as the hemispheric means the expressions for τ_x and τ_y are linear and the requirement for the $\sin\phi$ weighting is explicitly evident on considering the spectral representation of these terms.]

The quantities U and V appearing in expressions (13) to (19) are derived via the simple linear relationship given by (9), which may be rewritten as

$$U = -\frac{\cos\phi}{a}\frac{\partial\psi}{\partial\phi} + \frac{1}{a}\frac{\partial\chi}{\partial\lambda} \quad (21)$$

$$V = -\frac{1}{a}\frac{\partial\psi}{\partial\lambda} + \frac{\cos\phi}{a}\frac{\partial\chi}{\partial\phi}. \quad (22)$$

The prognostic equations (13) to (16) and the diagnostics (4), (11), (21), and (22) constitute the formulation appropriate for the present study. These equations retain the character of the form suggested in I, i.e., the derived equations of vorticity and divergence are formulated so that nonlinear products are formed prior to differentiation. The truncation of the spectral representation of these equations is straightforward as all of the prognostic variables are scalars.

3. The equations of motion in spectral form

The model considers the prognostic variables of ψ, χ, and T in terms of orthogonal spherical harmonics at each of five levels in the vertical; the diagnostic variables Φ, U, and V are similarly represented at these levels as in the prognostic q at the surface. The multilevel configuration, as schematically given in Fig. 1, considers five full levels at spacings of $\Delta\sigma = 0.2$ together with corresponding equispaced half-levels.

Truncated expansions for the prognostic and diagnostic variables are required as follows:

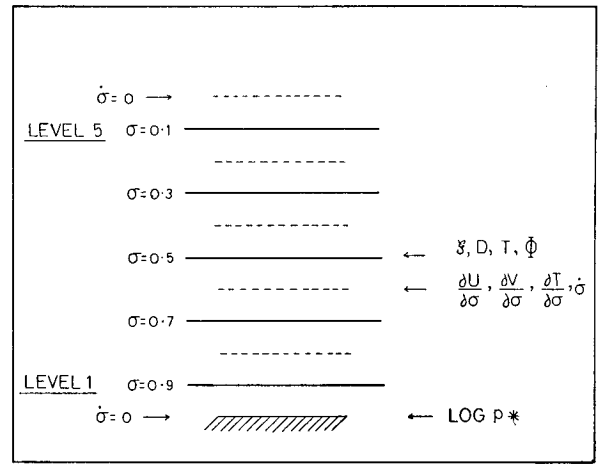

FIG. 1. Schematic of the disposition of the model levels with respect to the vertical coordinate σ. The half-levels denoted by dashed lines are equidistant in σ from the full levels.

$$\psi = a^2 \sum_{m=-J}^{+J} \sum_{l=|m|}^{|m|+J} \psi_l^m Y_l^m; \quad \chi = a^2 \sum_{m=-J}^{+J} \sum_{l=|m|}^{|m|+J} \chi_l^m Y_l^m$$

$$T = \sum_{m=-J}^{+J} \sum_{l=|m|}^{|m|+J} T_l^m Y_l^m; \quad q = \sum_{m=-J}^{+J} \sum_{l=|m|}^{|m|+J} q_l^m Y_l^m$$

$$U = a \sum_{m=-J}^{+J} \sum_{l=|m|}^{|m|+J+1} U_l^m Y_l^m; \quad V = a \sum_{m=-J}^{+J} \sum_{l=|m|}^{|m|+J+1} V_l^m Y_l^m$$

$$\Phi = a^2 \sum_{m=-J}^{+J} \sum_{l=|m|}^{|m|+J} \Phi_l^m Y_l^m, \quad (23)$$

where

a) the terms ψ_l^m and so forth denote time dependent generally complex expansion coefficients; the reality of the fields requires $(\psi_l^m)^* = (-)^m \psi_l^{-m}$ and so forth;
b) $Y_l^m = P_l^m(\sin\phi)e^{im\lambda}$; $P_l^m(\sin\phi)$ is an associated Legendre polynomial of the first kind normalized to unity; and
c) the wavenumber J denotes rhomboidal wavenumber truncation (Ellsaesser, 1966).

Diagnostic relationships for U_l^m and V_l^m as obtained from the linear relationships (21) and (22) are

$$U_l^m = (l-1)\epsilon_l^m \psi_{l-1}^m - (l+2)\epsilon_{l+1}^m \psi_{l+1}^m + im\chi_l^m \quad (24)$$

$$V_l^m = -(l-1)\epsilon_l^m \chi_{l-1}^m + (l+2)\epsilon_{l+1}^m \chi_{l+1}^m + im\psi_l^m, \quad (25)$$

where

$$\epsilon_l^m = \sqrt{(l^2-m^2)/(4l^2-1)}.$$

The hydrostatic relationship as given in (4) may be

expressed spectrally as

$$\frac{\partial \Phi_l^m}{\partial \sigma} = -\frac{R}{a^2}\frac{T_l^m}{\sigma}. \tag{26}$$

The spectral representation of nonlinear products occurring in the prognostic and diagnostic equations requires consideration of spectral grid transforms. The nonlinear products are evaluated on a latitude-longitude grid at each model level; these products then expressed as truncated Fourier series at each latitude circle are

$$\begin{aligned}
\xi U + \dot\sigma\frac{\partial V}{\partial \sigma} + \frac{RT'}{a}\cos\phi\frac{\partial q}{\partial \phi} - \frac{g}{p_*}\frac{\partial \tau_y}{\partial \sigma} &= a\sum_{m=-J}^{+J} A_m e^{im\lambda} \\
\xi V - \sigma\frac{\partial U}{\partial \sigma} - \frac{RT'}{a}\frac{\partial q}{\partial \lambda} + \frac{g}{p_*}\frac{\partial \tau_x}{\partial \sigma} &= a\sum_{m=-J}^{+J} B_m e^{im\lambda} \\
E &= a^2\sum_{m=-J}^{+J} E_m e^{im\lambda} \\
UT' &= a\sum_{m=-J}^{+J} F_m e^{im\lambda} \\
VT' &= a\sum_{m=-J}^{+J} G_m e^{im\lambda} \\
T'\nabla^2\chi + \dot\sigma\gamma + \frac{RT}{c_p}\{\overline{\nabla^2\chi} + (\mathbf{V}+\overline{\mathbf{V}})\cdot\nabla q\} &= \sum_{m=-J}^{+J} H_m e^{im\lambda} \\
\overline{\mathbf{V}}\cdot\nabla q &= \sum_{m=-J}^{+J} z_m e^{im\lambda}.
\end{aligned} \tag{27}$$

The diagnostic evaluation of $\dot\sigma$ is required only at grid points and is not subsequently expressed spectrally.

With additional representations given by

$$(\ )_l^m = \int_{-\pi/2}^{+\pi/2} (\ )_m P_l^m(\sin\phi)\cos\phi d\phi$$

and applied to E_m, H_m, and z_m, thereby yielding E_l^m, H_l^m, and z_l^m, the spectral amplitude tendencies for the streamfunction, velocity potential, temperature, and surface pressure (logarithm) are found to be

$$\begin{aligned}
-l(l+1)\frac{\partial \psi_l^m}{\partial t} = &-\int_{-\pi/2}^{+\pi/2}\frac{1}{\cos^2\phi}\left\{imA_m P_l^m(\sin\phi) - B_m\cos\phi\frac{\partial P_l^m(\sin\phi)}{\partial\phi}\right\}\cos\phi d\phi \\
&+2\Omega\{l(l-1)\epsilon_l^m\chi_{l-1}^m + (l+1)(l+2)\epsilon_{l+1}^m\chi_{l+1}^m - V_l^m\}
\end{aligned} \tag{28}$$

$$\begin{aligned}
-l(l+1)\frac{\partial \chi_l^m}{\partial t} = &\int_{-\pi/2}^{+\pi/2}\frac{1}{\cos^2\phi}\left\{imB_m P_l^m(\sin\phi) + A_m\cos\phi\frac{\partial P_l^m(\sin\phi)}{\partial\phi}\right\}\cos\phi d\phi \\
&-2\Omega\{l(l-1)\epsilon_l^m\psi_{l-1}^m + (l+1)(l+2)\epsilon_{l+1}^m\psi_{l+1}^m + U_l^m\} \\
&+l(l+1)\left(E_l^m + \Phi_l^m + \frac{RT_0}{a^2}q_l^m\right)
\end{aligned} \tag{29}$$

$$\begin{aligned}
\frac{\partial T_l^m}{\partial t} = &-\int_{-\pi/2}^{+\pi/2}\frac{1}{\cos^2\phi}\left\{imF_m P_l^m(\sin\phi) - G_m\cos\phi\frac{\partial P_l^m(\sin\phi)}{\partial\phi}\right\}\cos\phi d\phi \\
&+H_l^m
\end{aligned} \tag{30}$$

$$\frac{\partial q_l^m}{\partial t} = z_l^m - l(l+1)\overline{\chi_l^m}. \tag{31}$$

The integrals occurring in (28), (29), and (30) arise from the divergence and curl operators in (13), (14), and (15). The procedure of derivation of these spectral prognostics parallels the method detailed in I with respect to the free surface equations. The evaluation of the integrals proceeds via Gaussian quadrature and for this purpose the latitude circles are in fact Gaussian angles of latitude. This formulation facilitates computer coding as the nonlinear contributions to spectral tendencies may be accumulated successively at each Gaussian latitude (Eliasen *et al.*, 1970).

In evaluation of nonlinear products the fields transformed from the spectral to grid point domain, at the requisite Gaussian latitudes, are $\nabla^2\psi$, $\nabla^2\chi$, T, U, and V at each full level and q, $\partial q/\partial\lambda$, and $\cos\phi\partial q/\partial\phi$. The nonlinear products require evaluation of vertical derivatives and integrals; the values of $\dot\sigma$, $\partial U/\partial\sigma$, $\partial V/\partial\sigma$, $\partial T/\partial\sigma$, $\overline{\mathbf{V}}$, $\overline{\mathbf{V}}^\sigma$, $\overline{\nabla^2\chi}$, and $\overline{\nabla^2\chi}^\sigma$ are all evaluated by finite differencing at half-levels. The requisite full-level values are obtained upon averaging adjacent half-level values; where appropriate, the products (e.g., $\dot\sigma\partial U/\partial\sigma$) are evaluated at half-levels prior to averaging. Logarithmic variation of temperature between the first two full levels is assumed in defining $\partial T/\partial\sigma$ at the first full and half-levels.

The spectral amplitudes of the geopotential field are derived from vertical integration of (26); the topography, expressed spectrally, defines the lower limit of integration and successive full levels define the upper limit. The first two full-level temperatures are used to define a linear logarithmic dependence with respect to σ from the lower surface to the second full level for the purposes of this integration; above

the second full level the half-level temperature is the average of adjacent full-level values.

For the transform procedure to be equivalent to that in which spectral multiplications are considered analytically the grid point resolution must be sufficient to ensure alias free evaluation of all inverse transforms. As discussed in I, a grid of $\geqslant (5J+1)/2$ Gaussian angles of latitude and $\geqslant 3J+1$ equispaced longitudinal points is adequate for alias free evaluation of quadratic terms. It is to be noticed however that the nonlinear terms involving the vertical velocity $\dot{\sigma}\partial U/\partial\sigma$, $\dot{\sigma}\partial V/\partial\sigma$, and $\dot{\sigma}\gamma$ imply triplet products as $\dot{\sigma}$ itself has a quadratic dependence. In the model as presently described the grid resolution has been defined so as to provide alias free evaluation of quadratics only; this procedure appears to be satisfactory.

4. Semi-implicit time integration

The highly satisfactory performance of the semi-implicit time integration algorithm (Robert, 1969) as used in I strongly suggested its incorporation in the present model. The extension of the algorithm to the multilevel domain is non-trivial and the procedure designed for this model is detailed in the following.

Robert has extended his semi-implicit algorithm for use in a multi-level finite difference hemispheric model (Robert *et al.*, 1972); he also reports on semi-implicit integrations of a multi-level spectral model (Robert, 1970). In these models the thermodynamic equation is considered at half-levels and the semi-implicit algebra detailed by Robert is not as appropriate with the vertical disposition of variables where temperature is carried at full levels. Accordingly, the algorithm presented below differs from those referred to above; the present method may be broadly described as paralleling the free surface equations scheme with temperature replacing the free surface height.

Before proceeding with the description of the algorithm it is convenient to rewrite the spectral prognostics in a simpler form. The prognostics for the velocity potential (29), temperature (30) and surface pressure (logarithm) (31) may be rewritten after some manipulation as:

$$\frac{\partial D_l^m}{\partial t} = x_l^m + l(l+1)(\Phi_l^m + R'T_0 q_l^m) \tag{32}$$

$$\frac{\partial T_l^m}{\partial t} = y_l^m + \gamma_0(\overline{D}_l^m - \overline{D}_l^{m\sigma}) + \sigma\frac{\partial T_0}{\partial\sigma}\overline{D}_l^m \tag{33}$$

$$\frac{\partial q_l^m}{\partial t} = z_l^m + \overline{D}_l^m, \tag{34}$$

where $D_l^m = -l(l+1)\chi_l^m$, the quantities x_l^m, y_l^m, and z_l^m denote the spectral representation of the nonlinear terms and other terms not explicit here, and R' denotes R/a^2. The manipulation of the thermodynamic prognostic equation into this form requires extraction of the linear components, explicitly given in (33), from the term $\dot{\sigma}\gamma + RT/c_p\overline{\nabla^2\chi}$ which arises in the nonlinear contribution to the tendency. $\gamma = \gamma_0 + \gamma'$ and $T = T_0 + T'$ denote global mean values and the deviation from that mean. For clarity of presentation the superscript m and subscript l are implied in the following; in addition, matrix representation is employed with bold type denoting matrices.

The vertical integration of the hydrostatic relation (26) and evaluation of Φ at successive full levels may be expressed in matrix form as

$$\mathbf{\Phi} = R'\mathbf{A}\mathbf{T}. \tag{35}$$

$\mathbf{\Phi}$ and $\mathbf{T}$ denote column vectors of dimension given by the number of levels N; $\mathbf{A}$ is a square matrix of dimension $N\times N$ whose elements are as described in Appendix A.

The vertical integration and differencing required in the thermodynamic equation may also be written in matrix form and the temperature prognostics represented as

$$\frac{\partial \mathbf{T}}{\partial t} = \mathbf{y} + \Delta\sigma\mathbf{G}\mathbf{D}, \tag{36}$$

where $\mathbf{y}$ and $\mathbf{D}$ are N-dimensional column vectors, and the $\mathbf{G}$ matrix defines, as described in Appendix A, the finite difference representation of $\gamma_0(\overline{D}-\overline{D}^{\sigma}) + \sigma(\partial T_0/\partial\sigma)\overline{D}$.

Application of the operator $R'\mathbf{A}$ to both sides of (36) yields

$$\frac{\partial \mathbf{\Phi}}{\partial t} = R'\mathbf{A}\mathbf{y} + \Delta\sigma R'\mathbf{A}\mathbf{G}\mathbf{D}. \tag{37}$$

The divergence equation and surface pressure prognostic similarly represented are

$$\frac{\partial \mathbf{D}}{\partial t} = \mathbf{x} + l(l+1)(\mathbf{\Phi} + R'\mathbf{T}_0 q) \tag{38}$$

$$\frac{\partial q}{\partial t} = z + \Delta\sigma\mathbf{I}\mathbf{D}, \tag{39}$$

where, as indicated in Appendix A, $\mathbf{I}$ is the transpose of a unit vector of dimension N.

The finite time differencing of equations (37), (38), and (39) may now be defined in terms of the widely used centred (leap-frog) scheme and the semi-implicit operator, given by Robert (1969), as follows:

$$\mathbf{\Phi}^{\tau+1} = \mathbf{\Phi}^{\tau-1} + 2\Delta t R'\mathbf{A}\mathbf{y} + \Delta t\Delta\sigma R'\mathbf{A}\mathbf{G}(\mathbf{D}^{\tau+1} + \mathbf{D}^{\tau-1}), \tag{40}$$

$$\mathbf{D}^{\tau+1} = \mathbf{D}^{\tau-1} + 2\Delta t\mathbf{x} + \Delta t l(l+1)\{(\mathbf{\Phi}^{\tau+1} + \mathbf{\Phi}^{\tau-1}) + R'\mathbf{T}_0(q^{\tau+1} + q^{\tau-1})\}, \tag{41}$$

$$q^{\tau+1} = q^{\tau-1} + 2\Delta t z + \Delta t\Delta\sigma\mathbf{I}(\mathbf{D}^{\tau+1} + \mathbf{D}^{\tau-1}). \tag{42}$$

TABLE 1. Amplitude and phase speed of analytic streamfunction wave.

Level	24 Hours Ampli-tude km² sec⁻¹	24 Hours Av. phase speed deg. per day	96 Hours Ampli-tude km² sec⁻¹	96 Hours Av. phase speed deg. per day
$\sigma=0.1$	39.84	9.56	34.75	9.26
$\sigma=0.3$	39.84	9.23	38.19	9.10
$\sigma=0.5$	40.02	8.99	40.01	9.00
$\sigma=0.7$	40.19	8.86	40.87	8.98
$\sigma=0.9$	40.34	8.82	40.80	8.94

These three equations now embody three unknowns and may be solved. The procedure adopted is to substitute for $q^{\tau+1}$ and $\mathbf{\Phi}^{\tau+1}$ in (41) as follows

$$\mathbf{D}^{\tau+1}=\mathbf{D}^{\tau-1}+2\Delta t\mathbf{x}+\Delta t l(l+1)\{2\mathbf{\Phi}^{\tau-1}+2\Delta t R'\mathbf{A}\mathbf{y} +\Delta t\Delta\sigma R'\mathbf{A}\mathbf{G}(\mathbf{D}^{\tau+1}+\mathbf{D}^{\tau-1})\}+\Delta t l(l+1) \times R'\mathbf{T}_0\{2q^{\tau-1}+2\Delta t z+\Delta t\Delta\sigma\mathbf{I}(\mathbf{D}^{\tau+1}+\mathbf{D}^{\tau-1})\}. \quad (43)$$

Further arrangement yields, with $\mathbf{1}$, denoting a unit matrix

$$\{\mathbf{1}-\Delta t^2 l(l+1)R'\Delta\sigma(\mathbf{A}\mathbf{G}+\mathbf{T}_0\mathbf{I})\}\mathbf{D}^{\tau+1} =\{\mathbf{1}+\Delta t^2 l(l+1)R'\Delta\sigma(\mathbf{A}\mathbf{G}+\mathbf{T}_0\mathbf{I})\}\mathbf{D}^{\tau-1}+2\Delta t\mathbf{x} +2\Delta t l(l+1)\{\mathbf{\Phi}^{\tau-1}+\Delta t R'\mathbf{A}\mathbf{y}+R'(q^{\tau-1}+\Delta t z)\mathbf{T}_0\}. \quad (44)$$

The solution for $\mathbf{D}^{\tau+1}$ can be seen to involve the inversion of the coefficient matrix on the left-hand side of (44); in practice the solution is obtained by means of Gauss elimination and complete pivoting. With $\mathbf{D}^{\tau+1}$ available, $q^{\tau+1}$ is obtained from (42) and $\mathbf{T}^{\tau+1}$ is obtained most conveniently from (36) expressed as

$$\mathbf{T}^{\tau+1}=\mathbf{T}^{\tau-1}+2\Delta t\mathbf{y}+\Delta\sigma\Delta t\mathbf{G}\{\mathbf{D}^{\tau+1}+\mathbf{D}^{\tau-1}\}. \quad (45)$$

The prognostic sequence requires application of the above algorithm for each spectral degree of freedom; as the quantity $\mathbf{D}$ is generally complex, this requires $\sim 2J^2$ solutions via Gauss elimination per model time step.

5. Model computer coding

A computer code has been developed to numerically integrate the spectral tendency equations (28) to (31). The code employs the fast Fourier transform subroutines of Brenner (1969) and the procedures of Belusov (1962) for generating the associated Legendre polynomials (as in I).

The five-level $J=15$ model requires 13 min to perform a 24-hr ($\Delta t=3600$ sec) hemispheric integration on the Melbourne World Meteorological Centre IBM 360/65 computer; the model is coded in Fortran and employs the level-H compiler. The semi-implicit time step algorithm represents an overhead of $\sim 5\%$ per time step relative to an explicit time step scheme. The model is coded for global or hemispheric integrations at a maximum resolution of $J=15$ and requires 185 K bytes of core memory and little or no peripheral usage; in hemispheric integrations the hemispheres are considered to be identical and the computation time is accordingly half that of the global integration. The transform grid in $J=15$ hemispheric integrations comprises 20 Gaussian latitudes and 48 equispaced longitudes.

All calculations to be discussed have employed zero topography, i.e., the $\sigma=1$ surface defines mean sea-level.

6. Model integration with analytic initialization

A first evaluation of the model integrations employed an adaptation of the analytic initialization suggested by Phillips (1959) for use in free surface model integrations (as used in I). The model was initialized with the same analytic flow pattern at all levels, as isothermal throughout, and as inviscid, i.e., the dissipative surface drag was omitted as were also the subsequently described divergence dissipation (see Section 7. *a*) and sub-truncation-scale parameterization (see Section 7. *b*).

The detail of the analytic specification is given in Appendix B; it suffices to note here that the analytic non-divergent barotropic solution yields a wave travelling at a constant phase speed of 9.6° per day with constant wave amplitude. With this initialization the multilevel model would be expected to evolve initially as though barotropic and non-divergent with deviations arising as the model divergence grows and vertical shears develop. The model was integrated, in a hemispheric mode, at a resolution of $J=15$ to 96 hours via the semi-implicit scheme using one-hour time steps. The wavenumber 4 streamfunction amplitudes at 24 and 96 hr and the average phase speeds in these time intervals are given in Table 1; the initial streamfunction amplitude of wavenumber four at all levels was 40.23 km² sec⁻¹.

The amplitude and phase speed at 24 hr, averaged over the five levels, are 40.05 km² sec⁻¹ and 9.1° per day respectively. This response is considered satisfactory in terms of horizontal advection; the numerical phase speed is as might be anticipated from the free surface model behavior discussed in I, less than the analytic value. It is seen in Table 1 that the wave amplitude is maintained at lower levels while the phase speed approaches the analytic solution with increasing level height. ($J=15$ is considered an adequate resolution for such an analytic wave integration on the basis of the free surface integrations of Puri and Bourke (1974a). The highly oscillatory and truncation dependent behavior of $J=5$, as observed in the above-cited free surface integrations, persists also in the multilevel model.)

This analytic initialization has treated the atmosphere as adiabatic and inviscid and the extent to

which the model integrations satisfy, among others, principles of conservation of energy, angular momentum and mass, is of importance. The conservation principles may be expressed as constraints on the integrals over the mass field of the fluid of the quantities, given per unit mass, of

$$\text{Energy}=\frac{U^2+V^2}{2\cos^2\phi}+\Phi+c_vT$$

and

$$\text{Angular momentum}=a(U+\Omega a\cos^2\phi).$$

Conservation of mass is measured by the constancy of the mean surface pressure in the model.

The energy and angular momentum integrals may be expressed spectrally as

Energy/Unit mass

$$=\frac{a^2}{\sqrt{2}p_0{}^0}\int\sum_{m=-J}^{+J}\sum_{l=|m|}^{|m|+J}p_l{}^{m*}\left\{E_l{}^m+\Phi_l{}^m+\frac{c_v}{a^2}T_l{}^m\right\}\partial\sigma$$

Angular momentum/Unit mass

$$=\frac{a^2}{\sqrt{2}p_0{}^0}\left[\int\sum_{m=-J}^{+J}\sum_{l=|m|}^{|m|+J}p_l{}^{m*}U_l{}^m\partial\sigma+\Omega\left(\frac{2}{3}\sqrt{2}p_0{}^0-\frac{1}{3}\sqrt{\frac{8}{5}}p_2{}^0\right)\right].$$

For these diagnostic purposes its necessary to evaluate the spectral representation for p_*,

$$p_*=\sum_{m=-J}^{+J}\sum_{l=|m|}^{|m|+J}p_l{}^mY_l{}^m.$$

The amplitudes are obtained after a spectral to grid transformation of $\log p_*$, exponentiation and subsequent inverse transformation; this calculation is clearly more complex than just quadratic and is of course aliased in the spectral grid transform which is designed to yield alias free evaluation of quadratics.

The global integrals of total energy, angular momentum, and mass varied in the 96-hr period of integration by -0.013, $+0.170$ and -0.027 percent respectively; the angular momentum conservation ignores the constant contribution proportional to Ωa^2 which here is an order of magnitude larger than the other two contributing terms.[1]

[1] During the 96-hr period the changes in kinetic energy and potential energy relative to the initial total energy were $+0.008\%$ and -0.022% respectively. The potential to kinetic energy conversions do not balance exactly although further perspective on this aspect of model performance is obtained via integrations initialized with real data sets such as described in Section 8. With the model considered as non-dissipative and initialized from 00Z 3 November 1969 an integration to 96 hr ($J=15$ and $\Delta t=3600$ sec) yielded changes in kinetic and potential energy relative to the total initial energy of $+0.028\%$ and -0.049% respectively. On relaxing the constraint of a logarithmic dependence of temperature with respect to σ from the lower surface to the second full level and assuming an isothermal temperature dependence below the first full level a repeat calculation to 96 hr yielded changes of kinetic and potential energy relative to the total initial energy of $+0.029\%$ and -0.033%. The performance with the logarithmic constraint is clearly less satisfactory from the imbalance point of view but the dynamic significance of such imbalances is considered unimportant as a root-mean-square difference of the two prognosed 96-hr mean sea-level pressure fields is only 0.68 mb. Accordingly the more realistic logarithmic constraint has been employed throughout these studies. (The conversion imbalance in the analytic integration is not improved upon relaxing the logarithmic dependence and inserting an isothermal lower layer).

The degree to which the model satisfied the above conservation principles was considered satisfactory. The model formulation offers no guarantee of conservation such as in models expressed in the flux form and it is to be noted that the present spectral algebra admits aliasing via triple products in those terms involving vertical advection and via the spectral evaluation of the key diagnostic quantity p_* as mentioned above.

As with the free surface model integrations, described in I, there was no manifestation of a computational mode in time in 96-hr integrations; a one-sided forward step was employed upon commencement of the integration only.

7. Model integrations with Southern Hemisphere data initialization

The model has been initialized with spectral analyses of Southern Hemisphere data sets. For this purpose a spectral analysis code was developed whereby numerical analyses of the form used by the Melbourne World Meteorological Centre could be transformed to the spectral domain at each of the requisite σ levels.

The experimental integrations to be described have been initialized from Southern Hemisphere data sets from the GARP observing period of November 1969. The detail of the numerical analysis and subsequent spectral analysis is given in Appendix C. It suffices to note here that output from the spectral analysis consists of temperature and derived fields of vorticity and divergence together with the surface pressure (logarithm); all fields are expressed spectrally up to a resolution of $J=15$. As analyzed the divergent wind component cannot be considered seriously and it has been explicitly put to zero prior to all integrations.

The calculations have employed the semi-implicit time integration scheme with $\Delta t=3600$ sec; a forward (semi-implicit) time step was employed at $t=0$ and there was no requirement for suppression of a computational mode in these 48-hr integrations.

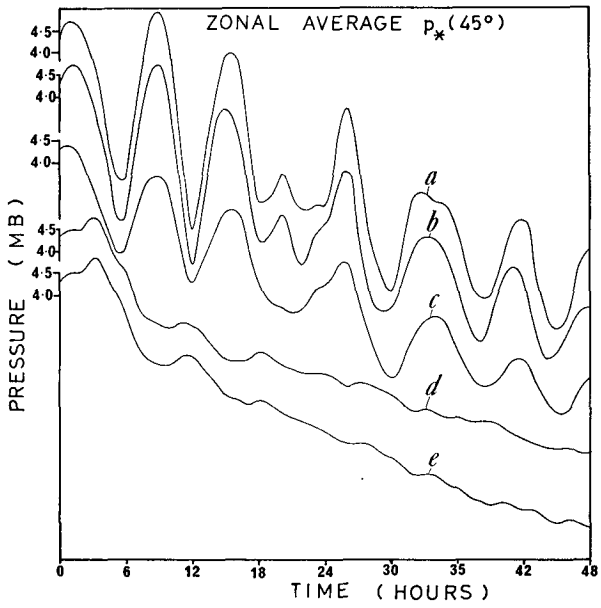

FIG. 2a. Zonal average of the surface pressure (relative to a hemispheric mean of 1009.5 mb) at latitude 45S as a function of time for 48-hr integrations with: (a) basic model; (b) divergence diffusion (after Sadourny, 1973); (c) dynamic initialization (after Nitta, 1969); (d) divergence dissipation on all scales; (e) divergence dissipation on zonal scales only.

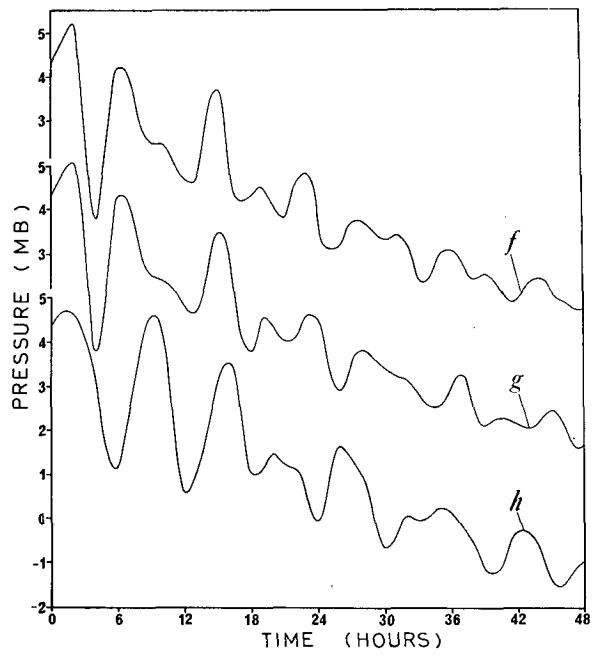

FIG. 2b. Zonal average of the surface pressure (relative to a hemispheric mean of 1009.5 mb) at latitude 45S as a function of time for 48-hr integrations with divergence dissipation ($K=0.50\times10^{-4}$ sec^{-1}), via (f) explicit time integration ($\Delta t=600$ sec); (g) semi-implicit time integration ($\Delta t=600$ sec); (h) semi-implicit time integration ($\Delta t=3600$ sec).

a. Model initialization

The atmospheric state specified by the numerical analysis can be considered as being in a state of gross dynamic balance. However, as commonly cited some care in initializing fields of primitive equation models is highly desirable if not essential.

The procedure of explicitly putting to zero the analysed divergence has been found in these integrations to be highly beneficial; growth of spurious large scale disturbances in low latitudes is prevented by this device. However, the characteristic inertia-gravity imbalance oscillations common to most primitive equation models (Haltiner, 1971) still persist.

In attempting to improve the initialization and remove spurious model responses, several procedures examined have been: A) dynamic initialization (Nitta, 1969); B) forced geostrophic adjustment via divergence diffusion after Sadourny (1973); and C) divergence dissipation.

The dynamic initialization scheme employed 24 cycles of the iterative algorithm ($\Delta t=600$ sec) given by Nitta (1969); at the completion of each cycle the surface pressure field was restored. For these iterative calculations only, the analyzed divergence was not put to zero.

Sadourny's forced geostrophic adjustment corresponds to the inclusion in the prognostics for momentum of a slightly nonlinear eddy diffusion term sensitive to the irrotational wind only. This is not simply incorporated in the spectral algebra and accordingly a linearization of Sadourny's scheme has been modeled; this linear form is equivalent to incorporating an additional term in the divergence prognostic equation (14) of the form $+K\nabla^2(\nabla^2\chi)$. A value of $K=7.5\times10^6$ m^2 sec^{-1} was employed but only on scales of motion for which the wavenumber $l\leqslant 15$; this restriction to larger scales facilitated the use of larger K values and was considered appropriate in view of the large scale nature of such oscillations.

The divergence dissipation algorithm has been arrived at the present study on the basis that a term of the form $-KD$ added to equation (14) would be more appropriate than a linearization of the term suggested by Sadourny; this divergence dissipation is not weighted in influence to the smaller scales of motion and should be more suitable in handling large scale model oscillations. Accordingly calculations incorporating divergence dissipation were performed.

Figure 2a displays the model response during 48-hr integrations from 00Z 3 November 1969; the zonal average of the surface pressure at 45S is plotted at hourly intervals.

Curve (a) denotes a calculation employing no special procedure other than zeroing of divergence prior to integration. Curve (b) denotes the calculation employing a linearization of Sadourny's scheme. The contribution of $K\nabla^2(\nabla^2\chi)$ to the divergent tendency is evaluated at time step $\tau-1$, i.e., via the simple forward time step, which is conditionally stable; the

value of $K=7.5\times10^6$ m^2 sec^{-1}. Curve (c) denotes a calculation initialized via dynamic initialization of 24 cycles with surface pressure restoration. Curve (d) denotes a calculation employing divergence dissipation. The contribution of $-KD$ to the divergent tendency is evaluated at time step $\tau+1$, i.e., via the backward implicit scheme which is unconditionally stable; the value of $K=5.0\times10^{-4}$ sec^{-1} for the first 12 time steps, 0.50×10^{-4} sec^{-1} for the next 12 time steps and thereafter 0.05×10^{-4} sec^{-1}. Curve (e) denotes a calculation as with curve (d) but with the dissipation of divergence applied only to tendencies of zonal divergence components.

All calculations of Fig. 2a employed semi-implicit integration with one-hour time steps. In addition, diffusive parameterization of sub-truncation-scale effects as described in the ensuing Section 7. *b* was also incorporated in these calculations.

The highly oscillatory response of the model integrations is evident from Fig. 2a, as is the comparative performance of the various procedures. The most satisfactory of these schemes in suppressing these spurious oscillations is that employing divergence dissipation, i.e., curve (d). The restriction of divergence dissipation to zonal scales produces only a minor deterioration in this improved model response.

On the basis of these results the inclusion of dissipation of divergence has been considered a satisfactory method of controlling spurious model oscillations of the type evident in Fig. 2a. There is no evidence to suggest that inclusion of such a term has adverse effects, although its full impact in the more recent version of the model, incorporating moist processes, has only been partially tested.

A comparison of verifications of the 24- and 48-hr predictions with divergence dissipation, curves (d) and (e) of Fig. 2a, indicated a quantitative loss of predictive skill upon restricting the divergence dissipation to zonal scales only. This suggests that there is scope for optimization of the scale dependence of this dissipative mechanism although this has not been studied here. (The time variation of the K value as specified is discontinuous and although it could more properly be made continuous it has been taken as for curve (d) in the following prediction experiments. It did not seem especially appropriate to dwell on such optimization as it was envisaged in the realistic use of the model for an analysis prognosis cycle that the requirement for the initially high K value would be relaxed.)

The restriction of divergence dissipation to zonal scales of divergence is equivalent to the incorporation of a term of the form $-K\bar{v}$, where $\bar{v}$ denotes the zonal average of meridional velocity, in a prognostic for the meridional wind; at the author's suggestion this parameterization has been included in the semi-spectral forecast model of Voice and Hunt (1974) and found to be quite effective in controlling spurious oscillations of the type discussed.

The amplitude of these oscillations is independent of the time integration algorithm and time step although the oscillation frequency is a function of time step. Figure 2b displays the model response, as in 2a, for three additional integrations.

Curve (f) denotes a 48-hr integration incorporating divergence dissipation on all scales. The contribution of $-KD$ is evaluated at $\tau+1$ and the value of $K=0.50\times10^{-4}$ sec^{-1}. An explicit time-step of $\Delta t=600$ sec was used for this integration.

Curve (g) denotes the same as curve (f) but with a semi-implicit time integration and $\Delta t=600$ sec. Curve (h) denotes the same as (g) but with $\Delta t=3600$ sec. The most pronounced difference in these latter three calculations, as shown in Fig. 2b, is the lower frequency of oscillation with the larger time step.

It is appropriate to present here a quantitative comparison of the semi-implicit and explicit (leap-frog) time integration algorithms. The root-mean-square differences, over the hemisphere, between 48-hr predictions of the mean-sea-level pressure fields via:

A) a semi-implicit scheme with $\Delta t=600$ sec and an explicit scheme with $\Delta t=600$ sec; and
B) a semi-implicit scheme with $\Delta t=3600$ sec [curve (d) of Fig. 2a] and a semi-implicit scheme with $\Delta t=600$ sec

were found to be 0.06 and 0.42 mb respectively. [These three integrations all employed the same divergence dissipation, i.e., as per curve (d) in Fig. 2a.] These quantitative comparisons confirmed the visual evaluation that the explicit/semi-implicit differences are meteorologically unimportant at 48 hr for these integrations.

b. Sub-truncation scale parameterization

In the course of the numerical prediction experiments it became evident that some parameterization was required to inhibit spectral blocking, i.e., growth of amplitude at small scales in the dynamic model variables (see Puri and Bourke, 1974a). Accordingly the commonly employed diffusive parameterization was incorporated in the prognostics for vorticity, temperature and surface pressure as follows:

$$\frac{\partial}{\partial t}\nabla^2\psi=\cdots+K_H\nabla^2(\nabla^2\psi+2\psi/a^2)$$

$$\frac{\partial T}{\partial t}=\cdots+K_H\nabla^2T$$

$$\frac{\partial q}{\partial t}=\cdots+K_H\nabla^2q.$$

There appeared to be no reason to include a diffusive term of the type described here in the divergence prognostic in view of the divergence dissipation parameterization described in Section 7. *a* above.

The value of K_H was here taken to be 2.5×10^5 m^2 sec^{-1} and the contribution to the tendencies somewhat arbitrarily was restricted to scales for which wave number $l>15$, i.e., for those components in the upper half of the rhomboid in $m\cdot l$ space. These diffusive contributions to tendencies were evaluated via the forward time-step scheme. It should be noted that there is no numerical requirement for the inclusion of these diffusive terms, i.e., the parameterization is not controlling numerical instabilities.

8. Southern Hemisphere numerical prediction

Numerical integrations were performed initializing from fifteen southern hemisphere analyses for 00Z 3 November 1969 to 00Z 17 November 1969. The integrations employed one-hour time steps, via the semi-implicit algorithm and the analyses, integrations, and verifications all employed spectral truncation of $J=15$.

An initial set of integrations, subsequently denoted as A, was performed without divergence dissipation or sub-truncation-scale parameterization and with the surface stress evaluated as linear terms, i.e., with the pre-bracket terms in (20) taken as hemispheric mean values. The second set of integrations, subsequently denoted as B, incorporated divergence dissipation, sub-truncation-scale parameterization and nonlinear surface stress.

While realizing the inadequacies of the data base of these analyses, an attempt has been made to quantify the predictive skill of the calculations. Accordingly 24- and 48-hr verifications have been extracted spectrally over the hemisphere; the average over 15 days for persistence and both the A and B integrations of the root-mean-square differences for the surface pressure, the streamfunction at $\sigma=0.5$ and the vorticity at $\sigma=0.5$ are presented in Table 2. It is evident in this table that the B integrations yield improvements over a persistence forecast both in the MSL and $\sigma=0.5$ fields and that they are superior to the A integrations.

TABLE 2. Root-mean-square differences time averaged.

	Mean sea-level pressure (mb)		Streamfunction* (km^2 sec^{-1}) $\sigma=0.5$		Vorticity (10^{-6} sec^{-1}) $\sigma=0.5$	
	24 hr	48 hr	24 hr	48 hr	24 hr	48 hr
Persistence	5.97	7.21	6.37	7.79	0.228	0.244
A	5.60	7.44	5.64	6.82	0.192	0.252
B	5.24	6.79	5.09	6.49	0.167	0.206

* The rms of the streamfunction in equivalent dekameters is obtained by multiplying the value in km^2 sec^{-1} by 0.7; this is based on the linear balance relation with f evaluated from an area average values of $\phi=30°$

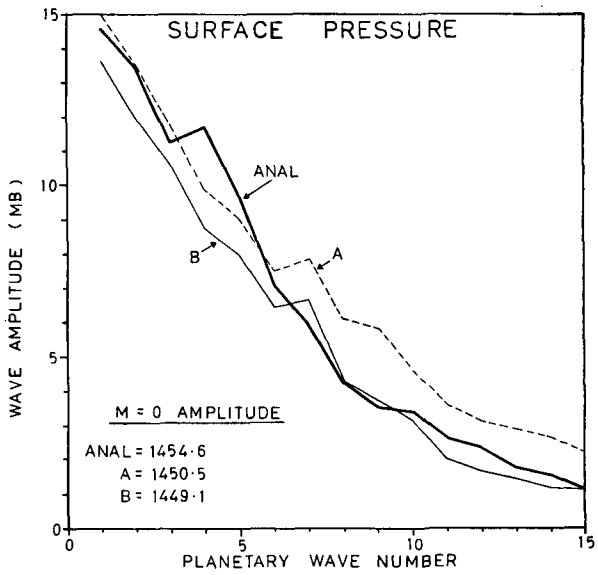

FIG. 3. Time-averaged (15 days) spectral amplitudes of surface pressure. The thick solid line denotes spectra of analyzed fields; the dashed line denotes spectra of the A integrations, the thin solid line denotes spectra of the B integrations.

Some indication of the predictive performance of the model, as viewed in the spectral domain is given by the time averaged planetary wave spectra of the 15 prognosed 48-hr fields from both the A and B integrations and of the 15 verifying analyses. The planetary wave amplitude is here taken as the wave amplitude at each wavenumber m summed over all l; the surface pressure planetary wave amplitudes, averaged over each of the fifteen fields are presented in Fig. 3.

A comparison of the spectra for the integrations A and B indicates that the inclusion of divergence dissipation and sub-truncation-scale parameterization constrains the smaller scale amplitudes to be akin to that of the observed. (The additional difference between the A and B integrations in the formulation of the surface stress is not considered important in the present context; it would be expected that the additional nonlinearity in the B integrations through the nonlinear formulation of the surface stress would if anything enhance the growth in amplitude at small scales). A loss of amplitude at larger scales is quite evident however in the B integrations. From a verification point of view both visually and quantitatively the under-estimation of large scale amplitude appears to be more acceptable than over-estimation of small scale wave amplitude. It is anticipated that the under-estimation of large scale wave amplitude may be less serious with increased resolution in the horizontal; Miyakoda *et al.* (1971) find improved maintenance and prediction of long waves with increasing horizontal

resolution and the truncation results of Puri and Bourke (1974a) also suggest that maintenance of large-scale planetary wave amplitude becomes much more effective with increasing horizontal resolution. In addition the requirement for sub-truncation-scale parameterization would be relaxed with higher resolution and the extent to which this parameterization reduces large scale amplitude would be similarly reduced.

The contribution of divergence dissipation to the loss of large scale amplitude has not been isolated. A more comprehensive evaluation of this formulation would be more properly undertaken as mentioned earlier in the context of an analysis-prognosis cycling scheme where the present requirement for an initially high dissipation coefficient could be relaxed; in the present experiments it seemed, as already described, appropriate and beneficial quantitatively to eliminate spurious model response via this procedure.

One example from the 15 prognoses (B model integrations) is given in Fig. 4; the MSL and the streamfunction and vorticity at $\sigma=0.5$ of the initial analysis (00Z 4 November 1969), of the verifying analysis (00Z 6 November 1969) and of the 48-hr model prognosis are shown. The quantitative verification for this 48-hr prognosis is given in Table 3 to indicate the performance relative to the averaged verifications of Table 2; quantitatively this prognosis gives slightly greater improvement relative to persistence than on average although the absolute error values are larger than on average.

The passage of a trough-ridge system across the southern Australian continent during the prognosis period is well captured by the model both at the surface and at the $\sigma=0.5$ level as seen in the stream lines and cyclonic vorticity centres; the prognosed ridging in the Great Australian Bight evident in all displayed fields is excessive. The blocking nature of the high pressure anticyclone in the New Zealand area is maintained as indicated by the persistent split current in the $\sigma=0.5$ streamfunction. The amplitude of the two troughs at MSL in the Indian ocean is reasonably maintained although the secondary development south of the African continent, evident in the vorticity analysis, is not captured. The subtropical ridge in general is reasonably well positioned although there is a loss of intensity, especially in the eastern Pacific. There is a tendency to high latitude ridging which could only be considered as highly coupled to the weakening of the subtropical ridge.

9. General comments

The integrations described in the present study have been conducted with a model simulating limited aspects of the atmospheric dynamics. The influence of moisture, radiative processes, topography and convection are the more notable omissions.

TABLE 3. Root-mean-square differences. 48-hr prognosis from 00 GMT 4 November 1969.

	Mean sea-level pressure (mb)	Streamfunction ($km^2\ sec^{-1}$) $\sigma=0.5$	Vorticity ($10^{-4}\ sec^{-1}$) $\sigma=0.5$
Persistence	8.16	8.83	0.280
Model B	7.26	7.12	0.233

There is in principle no guarantee that the model as described will maintain static stability. Indeed in the course of some of these integrations the numerical value of the static stability was seen to have negative excursions at several grid points towards the latter stages of the 48-hr period; this effect was a little more pronounced upon the inclusion of divergence dissipation. However, from the point of view of numerical model stability the onset of static instability was not of any real significance; in fact model integrations to 12 days from 00Z 3 November 1969 were numerically well behaved although becoming unacceptable synoptically. Phillips (1970) has noted that static instability in a hydrostatic atmosphere is unbounded and here the synoptic deterioration of a 12-day integration although slow is interpreted partly in terms of an inevitable increase of static instability in the model.

The requirement for a surface stress in the model was apparent in integrations beyond 3 or 4 days; the surface stress inhibits over-intensification of systems as manifest in the MSL charts and prevents consequent excess growth of kinetic energy at the lowest model levels.

A moisture prognostic including a precipitation calculation and parameterization of dry and moist convective adjustment has been included following the scheme of Manabe *et al.* (1965) and experiments with the moist version of the model are currently in process (Puri and Bourke, 1974b).

Numerical integrations including topography and via the semi-implicit algorithm ($\Delta t=3600$ sec, $J=15$ from 00Z 3 November 1969) have been performed. The topography employed is rather smoothed and is expressed spectrally (McAvaney, 1973); integrations to 96 hr are numerically well behaved although the topographical influence on prognosis detail has not been evaluated as yet.

Global model integrations have been performed initializing from data sets for December 1967 as used and made available by Baumhefner (1972); these integrations will be reported upon in the near future.

10. Conclusions

The formulation of a primitive equations multi-level spectral model of the atmosphere has been presented extending the previously reported approach of the

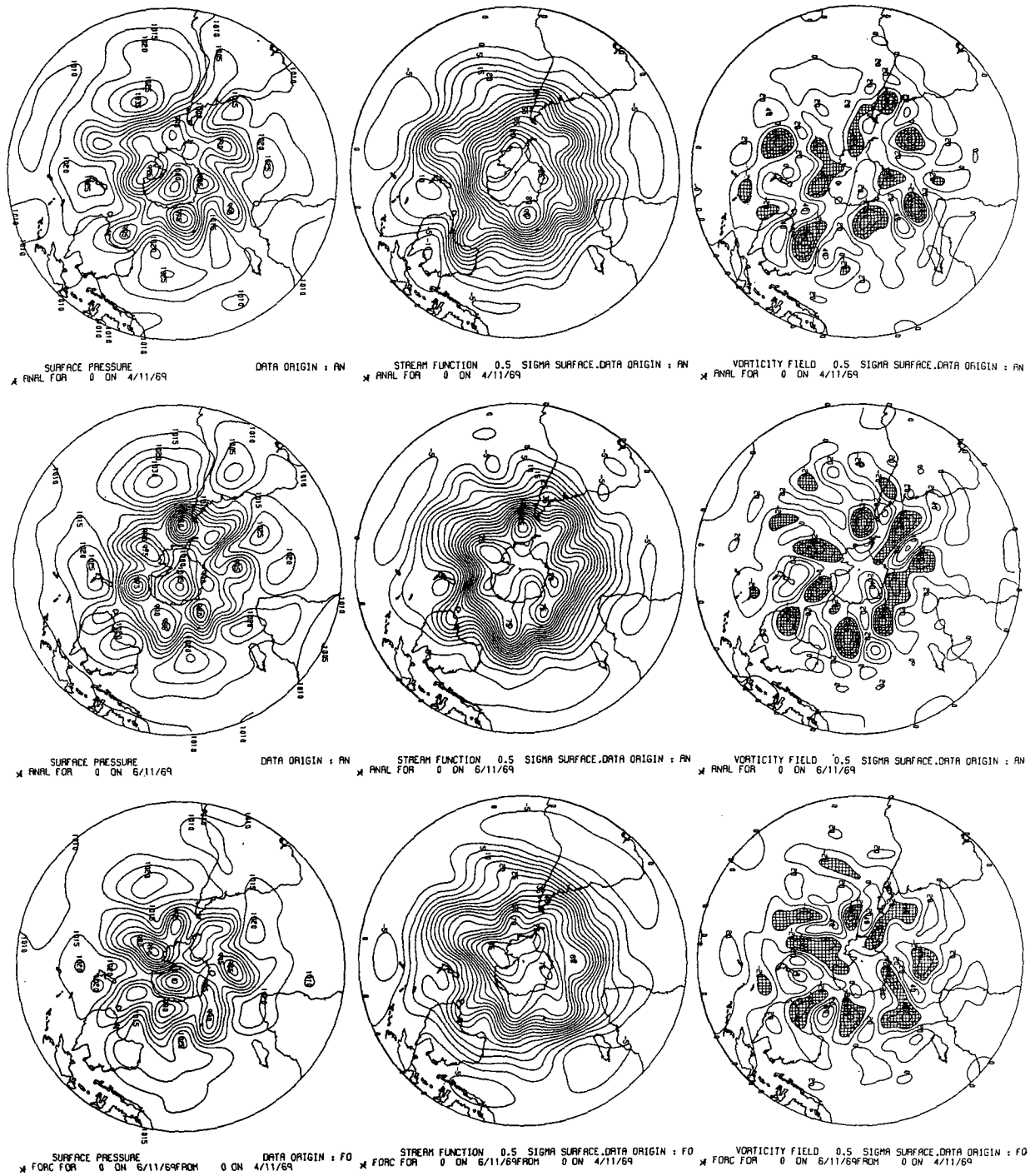

FIG. 4. An example of a 48-hr prognosis. From left to right the fields displayed are mean sea level pressure, the $\sigma=0.5$ stream-function and $\sigma=0.5$ vorticity; from top to bottom the fields are the initial analyses for 00Z 4 November 1969, the verifying analyses for 00Z 6 November 1969 and the 48-hr numerically predicted fields for 00Z 6 November 1969. Cross-hatching of vorticity denotes cyclonic centres with vorticity $\leq -0.20\times10^{-4}$ sec^{-1}.

author employing vorticity and divergence as dynamic variables.

An algorithm to incorporate the semi-implicit time integration scheme has been presented and it is found to be meteorologically equivalent to explicit time integration at least to 48 hr. It is implemented with little computational overhead thereby greatly enhancing the model efficiency.

The suggested analytic initialization provided a procedure for establishing model performance with respect to horizontal advection and to conservation of mass, angular momentum, and total energy. The conservation of these quantities was considered to be satisfactorily maintained although the qualifications of footnote 1 with respect to energy conversions should be noted.

Integrations with Southern Hemispheric meteorological data sets have been performed and a simple initialization combined with divergence dissipation has been shown to be an effective means of controlling a commonly cited but spurious and undesirable model response.

The detailed verifications of 15 prognoses have shown on average improvements over persistence for the Southern Hemisphere at 24 and 48 hr; this quantitative gain in predictive skill is visually identifiable, as in the prognosis example presented, and the model predictions are meteorologically informative and useful. The efficiency of the model is such that it could be readily implemented operationally.

Acknowledgments. The author gratefully acknowledges the assistance of Mr. R. L. Thurling; his expert programming of the spectral analysis, spectral display and model interface codes were essential to the completion of these studies.

The author thanks Mr. G. Kelly for making available the digitized GARP data sets and Mr. R. S. Seaman for generating the numerical grid point analyses. Thanks are also due to Mr. P. F. Noar for discussion of the synoptic performance of the model and to Drs. K. Puri, B. McAvaney and D. Anderson for continued interest and informative discussion of this work.

The global data sets referred to were kindly made available by Mr. D. Baumhefner of the National Center for Atmospheric Research (NCAR).

APPENDIX A

1) The geopotential may be obtained from vertical integration of the hydrostatic equation; the model requires geopotential values at full levels and the temperature dependence below the lowest full level thus requires specification. A linear logarithmic dependence with respect to σ is assumed between the lowest two full levels and the temperature dependence below the lowest full level is obtained from logarithmic extrapolation to the ground.

The dependence of T on σ in the range of levels 1 to 2 is defined as $T=c+b\ln\sigma$; c and b may then be found from

$$T_2=c+b\ln\sigma_2$$
$$T_1=c+b\ln\sigma_1.$$

With this representation of T up to level 2 the hydrostatic relation may be written as:

$$\frac{\partial\Phi}{\partial\ln\sigma}=-R(c+b\ln\sigma)$$

and Φ_i for $i=1$ and 2 then obtained as:

$$\Phi_i=\frac{-R\ln\sigma_i}{\ln\sigma_1/\sigma_2}\left[\left\{\frac{\ln\sigma_i}{2}-\ln\sigma_2\right\}T_1+T_2\left\{\ln\sigma_1-\frac{\ln\sigma_i}{2}\right\}\right].$$

Above level 2 the temperature between successive levels is simply averaged and Φ_i for $i>2$ obtained as

$$\Phi_i-\Phi_{i-1}=-R\frac{T_i+T_{i-1}}{2}\ln(\sigma_i/\sigma_{i-1}).$$

Further manipulation of these expressions allows matrix representation of the form

$$\mathbf{\Phi}=R\mathbf{A}\mathbf{T}$$

with the elements of $\mathbf{A}$ obtained as shown. [If topography, denoted by Φ_* is to be considered

$$\mathbf{\Phi}=R\mathbf{A}\mathbf{T}+\Phi_*\mathbf{I}^*$$

where $\mathbf{I}^*$ denotes a unit vector of dimension N. This only introduces modification to the implied definition of $\mathbf{x}$ in (38).]

2) The quantity $\gamma_0(\overline{D}-\overline{D}^\sigma)+\sigma\partial T_0/\partial\sigma\overline{D}$ as evaluated at each level using finite differences may be represented in matrix form. The following detail considers the simplest case of uniform spacing of levels in the vertical.

Finite-difference representation of vertical integration, as defined in (12), yields at level j

$$(\overline{D}-\overline{D}^\sigma)_j=\Delta\sigma\sum_{i=j}^{N}D_i-\Delta\sigma\frac{D_j}{2},$$

where

$$\overline{D}=\Delta\sigma\sum_{i=1}^{N}D_i,$$

and thus the required expression may be written at each level as

$$\Delta\sigma\left[(\gamma_0)_j\left(-\frac{D_j}{2}+\sum_{i=j}^{N}D_i\right)+\sigma_j\left(\frac{\partial T_0}{\partial\sigma}\right)_j\sum_{i=1}^{N}D_i\right].$$

Regrouping, this reduces to:

$$\Delta\sigma\left\{\left[\left(\frac{\gamma_0}{2}\right)_j+\sigma_j\left(\frac{\partial T_0}{\partial\sigma}\right)_j\right]D_j+\left[(\gamma_0)_j+\sigma_j\left(\frac{\partial T_0}{\partial\sigma}\right)_j\right]\sum_{i=j+1}^{N}D_i\ {}_{(j<N)}+\sigma_j\left(\frac{\partial T_0}{\partial\sigma}\right)_j\sum_{i=1}^{j-1}D_i\ {}_{(j>1)}\right\}.$$

Denoting $\sigma_j(\partial T/\partial\sigma)_j$ as b_j the term $\gamma_0(\overline{D}-\overline{D}^\sigma)+\sigma\partial T_0/\partial\sigma\overline{D}$ in matrix form may be expressed as $\Delta\sigma\mathbf{G}\mathbf{D}$ where the elements of the $N\times N$ matrix are

seen from above to be

$$\mathbf{G}=\begin{bmatrix} \left(\frac{\gamma_0}{2}\right)_1+b_1 & (\gamma_0)_1+b_1 & (\gamma_0)_1+b_1 & (\gamma_0)_1+b_1 & (\gamma_0)_1+b_1 \\ b_2 & \left(\frac{\gamma_0}{2}\right)_2+b_2 & (\gamma_0)_2+b_2 & (\gamma_0)_2+b_2 & (\gamma_0)_2+b_2 \\ b_3 & b_3 & \left(\frac{\gamma_0}{2}\right)_3+b_3 & (\gamma_0)_3+b_3 & (\gamma_0)_3+b_3 \\ b_4 & b_4 & b_4 & \left(\frac{\gamma_0}{2}\right)_4+b_4 & (\gamma_0)_4+b_4 \\ b_5 & b_5 & b_5 & b_5 & \left(\frac{\gamma_0}{2}\right)_5+b_5 \end{bmatrix}.$$

3) The quantity $\overline{D}$ occurring in the surface pressure prognostic is approximated as

$$\overline{D}=\Delta\sigma\sum_{i=1}^{N} D,$$

where $\Delta\sigma$ indicates the simplest case of uniform level spacing in the vertical. In matrix form the above becomes:

$$\overline{D}=\Delta\sigma\mathbf{ID}$$

where $\mathbf{I}$ is a row matrix of dimension N with elements of unity, i.e., the transpose of a unit vector.

APPENDIX B

Analytic Initialization

The Phillips streamfunction is given by

$$\psi=-a^2\omega\sin\phi+a^2\kappa\cos^R\phi\cos R\lambda.$$

For the present purposes the values chosen are as used in I and by Grimmer and Shaw (1967):

$$\omega=\kappa=\frac{\Omega}{10}\quad\text{and}\quad R=4.$$

The non-divergent analytic phase speed as given by Phillips is

$$\nu=\{R(R+3)\omega-2\Omega\}/(R+1)(R+2)=9.6^\circ\text{ per day.}$$

It remains to define an isothermal atmospheric temperature $T=266.4$ K and the mean surface pressure as 1000 mb. A balance condition may be obtained from (32) as follows

$$(\text{for } l>0)\ \frac{\partial D}{\partial t}=0=x_l^m+l(l+1)(\Phi_l^m+R'T_0q_l^m),$$

where Φ_l^m is initially zero and q_l^m may be thereby diagnosed. This diagnostic parallels the analytic expression for the mass field given by Phillips provided the nonlinearity of x_l^m is resolved.

The amplitude referred to in Table 1 is the quantity ψ_5^4 in units of km^2 sec^{-1}; the above Phillips streamfunction may be equivalently written in terms of $P_1^0(\sin\phi)$ and $P_5^{\pm4}(\sin\phi)e^{\pm i4\lambda}$.

APPENDIX C

The numerical analysis scheme is similar to that used by Gauntlett *et al.* (1972) and is the basis of numerical representation of the GARP November 1969 data sets. This numerical analysis scheme is operationally used at the Melbourne WMC.

The numerical analyses on a 47 × 47 stereographic projection of the Southern Hemisphere required:

i) digitization of the MSL and 500-mb geopotential analyses as drawn up by Phillpot *et al.* (1971);
ii) all available conventional data; and
iii) preliminary guess fields of:
   a) individual thickness and temperature below 500 mb from implied 1000–500 mb thickness and climatological statistics for latitudes poleward of 15S;
   b) individual thickness and temperature above 500 mb obtained statistically by extrapolation from 500 mb for latitudes poleward of 15S (Seaman, 1972);
   c) climatological specification of winds and temperatures equatorward of 15S and gradient/geostrophic specification of winds poleward of 25S; between 15S and 25S a weighted combination of climatology and gradient geostrophy to specify the winds.

The numerical analysis scheme provides at standard levels temperature, winds, and surface pressure.

Spectral analyses of these fields are obtained by:

i) horizontal interpolation to a latitude-longitude grid with the latitudes chosen as Gaussian angles;
ii) vertical interpolation to the requisite σ levels; and
iii) Fourier and associated Legendre transforms of these grid point fields.

The fields of temperature and surface pressure, vorticity and divergence are thus obtainable in spectral form. The derived wind fields are obtained by evaluating the spectral representation of:

$$\text{i)} \quad \xi = \frac{1}{a\cos^2\phi}\left(\frac{\partial V}{\partial \phi} - \cos\phi \frac{\partial U}{\partial \phi}\right);$$

and

$$\text{ii)} \quad D = \frac{1}{a\cos^2\phi}\left(\frac{\partial U}{\partial \lambda} + \cos\phi \frac{\partial V}{\partial \phi}\right).$$

U and V here are of course the numerically analyzed eastward and northward wind respectively weighted by cos(latitude).

Spectral analyses were thus obtained for the 17 days 00Z 3 November 1969 through to 00Z 19 November 1969; these analyses defined spectral amplitudes to a resolution $J=15$.

REFERENCES

Baer, F., and F. N. Alyea, 1971: Effects of spectral truncation on general circulation and long range prediction. *J. Atmos. Sci.*, **28**, 457–480.

Baumhefner, D. P., 1972: Further experimentation with an imposed southern boundary for large scale numerical weather prediction. *J. Atmos. Sci.*, **29**, 768–772.

Belusov, S. L., 1962: *Tables of Normalized Associated Legendre Polynomials*. Elmsford, N. Y., Pergamon Press, 379 pp.

Bourke, W., 1972: An efficient one-level primitive equation spectral model. *Mon. Wea. Rev.*, **100**, 683–689.

Brenner, N., 1969: Cooley-Tukey Fast Fourier Transform codes. File No. System 360-20, Contributed Program No. 360D-13.4.001, Systems Reference Library, IBM Corporation, New York.

Eliasen, E., B. Machenhauer, and E. Rasmussen, 1970: On a numerical method for integration of the hydrodynamical equations with a spectral representation of the horizontal fields. Institute of Theoretical Meteorology, University of Copenhagen, Report No. 2.

Ellsaesser, H. W., 1966: Evaluation of spectral versus grid methods of hemispheric numerical weather prediction. *J. Appl. Meteor.*, **5**, 246–262.

Gauntlett, D. J., R. S. Seaman, W. R. Kinninmonth, and J. C. Langford, 1972: An operational evaluation of a numerical analysis-prognosis system for the southern hemisphere. *Australian Meteor. Mag.*, **20**, 61–82.

Grimmer, M., and D. S. Shaw, 1967: Energy preserving integrations on the sphere. *Quart. J. Roy. Meteor. Soc.*, **93**, 337–349.

Haltiner, G. J., 1971: *Numerical Weather Prediction*. John Wiley & Sons, Inc., (p. 257), 317 pp.

Kikuchi, Y., 1969: Numerical simulation of the blocking process. *J. Meteor. Soc. Japan*, **47**, 29–54.

McAvaney, B., 1973: Spherical harmonic analysis of the earth's topography. (Unpublished).

Machenhauer, B., and R. Daley, 1972: A baroclinic primitive equation model with a spectral representation in three dimensions. Institute of Theoretical Meteorology, University of Copenhagen, Report No. 4.

——, and E. Rasmussen, 1972: On the integration of the spectral hydrodynamical equations by a transform method. Institute of Theoretical Meteorology, University of Copenhagen, Report No. 3.

Manabe, S., J. Smagorinsky, and R. F. Strickler, 1965: Simulated climatology of a general circulation model with a hydrologic cycle. *Mon. Wea. Rev.*, **93**, 769–798.

Miyakoda, K., R. F. Strickler, C. J. Nappo, P. L. Baker, and G. D. Hembree, 1971: The effect of horizontal grid resolution in an atmospheric circulation model. *J. Atmos. Sci.*, **28**, 481–499.

Nitta, T., 1969: Initialization and analysis for the primitive equation model. *Proc. WMO/IUGG Symposium on numerical weather prediction, Tokyo, 1968*. Japan Meteorological Agency, Tokyo.

Orszag, S. A., 1970: Transform method for calculation of vector coupled sums: Application to the spectral form of the vorticity equation. *J. Atmos. Sci.*, **27**, 890–895.

Phillips, N. A., 1959: Numerical integrations of the primitive equations on the hemisphere. *Mon. Wea. Rev.*, **87**, 333–345.

——, 1970: Models for weather prediction. *Annual Review of Fluid Mechanics*, **2**, 251–292. Annual Reviews, Inc.

Phillpot, H. R., P. G. Price, A. B. Neal, and F. A. Lajoie, 1971: GARP basic data set analysis project. The first experiment—November 1969. *Australian Meteor. Mag.*, **19**, 48–81.

Puri, K., and W. Bourke, 1974a: Implications of horizontal resolution in spectral model integrations. *Mon. Wea. Rev.*, **102**, 333–347.

——, and ——, 1974b: (Unpublished).

Robert, A. J., 1966: The integration of a low-order spectral form of the primitive meteorological equations. *J. Meteor. Soc. Japan*, **44**, 237–245.

——, 1969: Integration of a spectral model of the atmosphere by the implicit method. *Proc. WMO/IUGG Symposium on Numerical Weather Prediction, Tokyo*, 26 November–4 December 1968. Japan Meteorological Agency, Tokyo.

——, 1970: Forecast experiments with a spectral model. *Proc. Eighth Stanstead Seminar, Publication in Meteorology No. 97*. McGill University, Montreal.

——, J. Henderson, and C. Turnbull, 1972: An implicit time integration scheme for baroclinic models of the atmosphere. *Mon. Wea. Rev.*, **100**, 329–335.

Sadourny, R., 1973: Forced geostrophic adjustment in large scale flow. (Unpublished).

Seaman, R. S., 1972: Stability correlations and their application to objective analyses. *Australian Meteor. Mag.*, **20**, 83–103.

Voice, M. E., and B. G. Hunt, 1974: Private communication.